Effects of viscous shear stress on thermoregulation of electronics. Transient free convection in diode enclosures induced by discrete heat bands under constant heat flux

A. Baïri

Accepted Manuscript

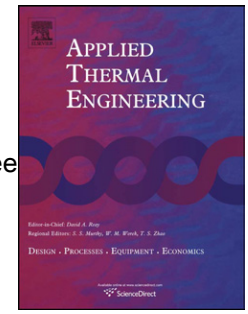

Title: Effects of viscous shear stress on thermoregulation of electronics. Transient free convection in diode enclosures induced by discrete heat bands under constant heat flux

Authors: A. Baïri

PII: S1359-4311(11)00319-X

DOI: 10.1016/j.applthermaleng.2011.06.009

Reference: ATE 3604

To appear in: *Applied Thermal Engineering*

Received Date: 22 January 2011

Revised Date: 14 April 2011

Accepted Date: 6 June 2011

Please cite this article as: A. Baïri. Effects of viscous shear stress on thermoregulation of electronics. Transient free convection in diode enclosures induced by discrete heat bands under constant heat flux, Applied Thermal Engineering (2011), doi: 10.1016/j.applthermaleng.2011.06.009

Effects of viscous shear stress on thermoregulation of electronics. Transient free convection in diode enclosures induced by discrete heat bands under constant heat flux

A. Baïri

Université Paris Ouest, LTIE-GTE EA 4415
50, rue de Sèvres, F-92410 Ville d'Avray, France

abairi@u-paris10.fr, bairi.a@gmail.com

Abstract

Thermal and dynamic phenomena that occur in the immediate vicinity of electronic components during operation generate viscous shear stresses due to velocity gradients. When thermocouples used for thermal regulation of these assemblies are installed in this environment, temperature measurements may be erroneous. It is therefore essential to take into account viscous effects in the boundary layer when dealing with thermal control of electronics subjected to natural convection. These phenomena are particularly pronounced and complex when generation of heat at the active wall is not uniform. That is the case for the real device treated in this work. The natural convective flow is generated by a vertical wall composed by alternated adiabatic and heated bands under constant heat flux, representing a working electronic equipment. The 2D transient boundary layer near the vertical active hot wall of parallelogram-shaped enclosures is treated in order to determine the viscous shear stress. Results are obtained by numerical approach using the finite volume method. Many geometrical configurations are treated while varying the inclination angle of the top and bottom passive adiabatic walls. The very different local distributions of viscous shear stresses and vertical thermal gradients confirm the necessity to take them into account to properly install the sensors used for thermoregulation.

Keywords

Heat transfer, thermal shear viscous stresses, electronic equipment, transient natural convection, diode cavities

Nomenclature

a	thermal diffusivity of the air (m^2s^{-1})
C	specific heat ($J\ kg^{-1}K^{-1}$)
D	dissipation number based on the height of the band H' (-)
Fo	Fourier number (-)
g	acceleration of the gravity ($m\ s^{-2}$)
H	height of the cavity; distance between the hot and cold walls (m)
H'	height of the hot band; $H'= H/5$ (m)
n^*	dimensionless local normal to the top and bottom passive walls (-)
p	pressure (Pa)

p^*	dimensionless pressure (-)
Pr	Prandtl number (-)
Ra	Rayleigh number (-)
t	time (s)
t^*	dimensionless time (-)
T	local temperature (K)
T^*	dimensionless temperature (-)
T_0	initial uniform temperature of the whole system (K)
T_c	temperature of the cold wall (K)
T_h	local instantaneous temperature at the hot active band (K)
u,v	flow velocity components in x and y directions respectively (m s^{-1})
u^*,v^*	dimensionless flow velocity components in x and y directions respectively (-)
W	depth of the hot and cold active walls (m)
x,x',y,z	Cartesian coordinates (m)
x^*,y^*,z^*	dimensionless Cartesian coordinates (-)

Greek symbols

α	inclination angle of the cavity (°)
β	expansion coefficient of the air (K^{-1})
∇^2	Laplacian operator
φ	heat flux at hot band (Wm^{-2})
λ	thermal conductivity of the air ($Wm^{-1}K^{-1}$)
μ	dynamic viscosity of the air (Pa s)
ρ	density of the air (kg m^{-3})
τ	viscous shear stress at the hot wall (Pa)
τ^*	dimensionless viscous shear stress at the hot wall (-)
$\overline{\tau_i^*}$	average dimensionless viscous shear stress at the i^{th} hot band (-)
$\overline{\tau^*}$	average dimensionless viscous shear stress at the hot wall (-)

1. Introduction

Thermal cases in electronic engineering are widely treated in the literature due to their industrial importance. Modern equipments are often based on a high miniaturization, are installed in more and more small volumes and dissipate a power density increasingly important. This leads to thermal states which may be incompatible with normal operation if their sizing is not correctly devised and if the design does not take into account all the thermal effects. Studies in this domain are nowadays most often done by thermal simulation, using codes that take into account the dynamic and thermal aspects of the flow, associated with space requirements and the power of the assembly. Joshi et al. [1] point out the challenges facing the thermal community when designing and optimizing electronic packages. Moghaddam et al. [2] evaluate some analytical heat transfer models for thermal design of electronic equipments and present a model for calculation of the heat flux and junction temperatures in a multi-chip module. Zhu et al. [3] take into account the effects of the fluid flow on the sensors for the development of a micromachined inertial gas sensor based on heat

convection. Besides that, several geometric configurations of the active hot wall are considered in the literature associated to different enclosure configurations as the octogonal one treated by Saha et al. [4] and several others devoted to natural convection as [5-8] among the latest. In electronic engineering, thermal control equipment often requires the use of thermocouples near the active hot wall. Measurement errors can be made if the effects of the local flow on the junctions of these sensors are not taken into account. It is then necessary to examine the dynamic and thermal boundary layers. Phenomena due to natural convection can be more or less pronounced, complex and diverse. Several physical parameters affect the nature of the flow. Among the most important are the heat power, the geometry and dimensions of the enclosure in which the equipment is located, the thermal boundary conditions and the arrangement of active walls relative to the gravity field. Convective exchanges are quantitatively and qualitatively different depending on the time elapsed since the power-on of the equipment. Temperature measured by the sensor at a specific time is thus very important for the thermal control system to take into account the real phenomena that occur. The present study is carried out in transient state to determine the instantaneous values of the main characteristics of the flow and their evolution up to the steady state.

The treated cavity has a particular shape. Two, hot and cold, active walls are opposite and remain vertical. They are separated by a distance equal to their height. The cold wall is isothermal while the hot one, representing the electronic equipment, is composed of three parallel bands generating a constant heat flux, separated by adiabatic bands. The channel of the cavity is considered as adiabatic. Its top and bottom walls are inclined at a given angle with respect to the horizontal, so lateral sections have a parallelogrammic shape. Values of inclination angles considered in the present work are 0º (square cavity), ±30° and ±60°, representative of the typical convective phenomena occurring in these particular cavities. Several geometric and thermal parameters have influence on the inner convection. These include the inclination angle of the passive walls, the temperature levels, the temperature difference between the active walls, the distance between them and their height. The thermal characteristics of the channel like thermal conductivity and emissivity and the thermophysical properties of the fluid obviously have a major influence on the flow and on the associated heat exchange. The natural flow is enhanced when the hot wall is lower than the cold one and diminished in the opposite situation, what confers this arrangement the quality of diode cavity in the convective sense of the term.

Natural convection for this type of cavity has been treated recently in some studies and applied to diverse engineering sectors. In solar thermal energy are used to limit the convective losses between the absorber and the cover of a flat plate solar collector [9]. Baïri [10] applies it to the field of building for the same geometrical configuration of the hot wall but with bands maintained isothermal. He presents the temperature fields and streamlines at some representative Fourier numbers with inclination angles varying between –60° to +60° in 15º-steps. The temporal evolution of the local and average Nusselt number at each band of the hot wall are also presented for all the treated configurations and can help to better understand the results of the present paper. The case of isothermal hot wall has been applied to on-board electronics by Baïri et al. [11,14]. It is also the case of the present study applied to the regulation of electronic assemblies. Some details concerning the transient convective heat transfer are provided in the numerical and experimental study [11]. Correlations of the *Nu-Ra* type for these configurations have been recently proposed by García de María et al. [12], while correlations for the case of the hot wall entirely isothermal are proposed by Baïri et al. [13]. Details on convective heat transfer for the case of imposed constant heat flux to the hot wall have been treated by Baïri et al [14]. The transient regime studied here completes these studies by examining the thermal and dynamic boundary layers near the hot wall. This allows to determine the viscous shear stresses and the vertical thermal gradients. The situations of

walls maintained either isothermal or subject to a constant flux density over the entire surface have been treated in steady state both theoretically and experimentally. Ostrach [15] and Gebhart [16,17] are among the first researches to solve these classical problems with the well-known similarity method taking into account the viscous dissipation. Nadim et al. [18] used the homotopy analysis method to solve the nonlinear differential equations of the free convection boundary layer on a vertical plate. Sillapää and Heinonen [19] examine the magnitude and effect of the variable shear stress on cylindrical surfaces. Based on the theory of similarity variables, the authors examine the evolution of the shear stress with time. Their interesting experimental study based on dynamic gravimetric gas mass flow shows that the variations of the shear stress can be seen as a change in the indication of a balance. Local distributions and average values of both the shear stress and the vertical temperature gradients are presented here at two representative Fourier numbers and different inclination angles. They show a significant difference depending on position and time. This confirms the importance of taking into account local phenomena to set up a correct arrangement of sensors used for the thermal regulation of electronic devices.

2. Physical model. Governing equations and calculation procedure

The parallelogram-shape air-filled cavity is represented in Fig. 1(a). Both hot and cold active walls (x=0; x=H) are vertical. The cold one is maintained isothermal at T_c while the hot one, represented in Fig. 1(b), consists of five superimposed discrete bands of the same height H'=H/5. Three bands (designed by 1, 2 and 3) are submitted to constant heat flux φ and they are separated by two adiabatic bands. Resulting local instantaneous temperature on this wall is denoted by $T_h(y,t)$. The channel of the cavity is considered as adiabatic. Flow inside the cavity, considered as 2D, is examined on the median plane ($z^* = z/W = 0.5$). Previous numerical studies and experimental measurements confirm that 3D effects are very limited, given the treated thermal boundary conditions and the depth W of the cavity. Governing equations of the considered problem are

$$\begin{cases} \dfrac{\partial u^*}{\partial x^*} + \dfrac{\partial v^*}{\partial y^*} = 0 \\ \dfrac{\partial u^*}{\partial t^*} + u^* \dfrac{\partial u^*}{\partial x^*} + v^* \dfrac{\partial u^*}{\partial y^*} = Pr \nabla^2 u^* \\ \dfrac{\partial v^*}{\partial t^*} + u^* \dfrac{\partial v^*}{\partial x^*} + v^* \dfrac{\partial v^*}{\partial y^*} = Pr \nabla^2 v^* + Ra\, Pr\, T^* - \dfrac{H'^3 g}{a^2}\left(1 + \dfrac{\partial p^*}{\partial y^*}\right) \\ \dfrac{\partial T^*}{\partial t^*} + u^* \dfrac{\partial T^*}{\partial x^*} + v^* \dfrac{\partial T^*}{\partial y^*} = \nabla^2 T^* + \dfrac{D}{Ra} \end{cases} \quad (1)$$

In this system, a is the thermal diffusivity, ∇^2 the Laplacian operator, while x^*, y^*, u^*, v^*, p^* and T^* are the dimensionless Cartesian coordinates, dimensionless velocity components, dimensionless pressure and dimensionless temperature respectively, defined as

$$x^* = \frac{x}{H};\ y^* = \frac{y}{H};\ u^* = \frac{u}{a/H'};\ v^* = \frac{v}{a/H'};\ p^* = \frac{p}{\rho g H'};\ T^* = \frac{T - T_c}{\frac{\varphi H'}{\lambda}} \quad (2)$$

The Rayleigh, Prandtl and Fourier numbers are defined as

$$Ra = \frac{g\beta H'^4 \rho}{\mu\lambda a}\varphi;\ Pr = \frac{\mu C}{\lambda};\ t^* = \frac{at}{H'^2} = Fo \tag{3}$$

The viscous dissipation term $\frac{D}{Ra}$ that appears in the energy equation represents the viscous heat generation and contains the dissipation number D based on the height of the band H'

$$D = \frac{g\beta H'}{C} \tag{4}$$

The boundary conditions (Fig. 1(c)) associated with the governing equations system (1) are: the no-slip condition applied to all walls of the cavity, adiabatic top and bottom passive walls, isothermal cold wall at temperature T_c , hot wall formed by three discrete bands under constant heat flux and two intermediate adiabatic ones

$$\begin{aligned}
&\left(u^* = v^*\right)_{\left[x^*=0\ ;\ 0\le y^*\le 1\right]\ ;\ \left[x^*=1\ ;\ \tan\alpha\le y^*\le 1+\tan\alpha\right]\ ;\ \left[0\le x^*\le 1\ ;\ y^*=x^*\tan\alpha\right]\ ;\ \left[0\le x^*\le 1\ ;\ y^*=1+x^*\tan\alpha\right]} = 0\\
&\left(\frac{\partial T^*}{\partial n^*}\right)_{\left[0\le x^*\le 1\ ;\ y^*=x^*\tan\alpha\right]\ ;\ \left[0\le x^*\le 1\ ;\ y^*=1+x^*\tan\alpha\right]} = 0\ ;\ n^* = n\ /H'\\
&T^*_{\left[x^*=1\ ;\ \tan\alpha\le y^*\le 1+x^*\tan\alpha\right]} = 0\\
&\left(\frac{\partial T^*}{\partial x^*}\right)_{\left[x^*=0\ ;\ 0\le y^*\le \frac{1}{5}\right]\ ;\ \left[x^*=0\ ;\ \frac{1}{5}\le y^*\le \frac{3}{5}\right]\ ;\ \left[x^*=0\ ;\ \frac{3}{5}\le y^*\le 1\right]} = -5\\
&\left(\frac{\partial T^*}{\partial x^*}\right)_{\left[x^*=0\ ;\ \frac{1}{5}\le y^*\le \frac{2}{5}\right]\ ;\ \left[x^*=0\ ;\ \frac{3}{5}\le y^*\le \frac{4}{5}\right]} = 0
\end{aligned} \tag{5}$$

Local viscous shear stress is calculated all along the hot wall $\tau = \tau_{x=0\ ,\ y}$ by using the absolute viscosity of the air μ and the local vertical velocity gradient

$$\tau = \mu\left(\frac{\partial v}{\partial x}\right)_{x=0} \tag{6}$$

whose dimensionless form is

$$\tau^* = \frac{\tau}{\frac{a\mu}{H'^2}} \tag{7}$$

Details concerning the numerical calculations and procedure are provided in [11,12]. They are carried out by means of the finite volume method presented in Patankar [20]. The cavity domain is discretised with a regular quadrangular mesh following *x*'- and *y*-direction. The mesh is finer near the hot wall in order to better reproduce the viscous effects and the thermal heat transfer in the boundary layer, which is the main objective of the present work. Particular attention was paid also to fluid zones between the hot wall bands to appreciate the details of

the local phenomena. The mesh near the top and bottom passive walls is finer than in the interior of the cavity in order to avoid computational difficulties due to deformation of the mesh. This optimization work is important because for some combinations involving large values of α and *Ra*, the computing time is very long but the precision is not necessarily better. The difficulties increase when studying the transient regime as in the present work. Moreover, to simplify the calculation procedure of the many treated cases, the number of meshes is chosen equal in both *x'*- and *y*- direction. The Nusselt number, which is representative of natural convection problems, is chosen as the main indicator for the accuracy of calculations. The maximum deviation allowed for *Nu* is of ±5% in transient regime and ±3% in steady state. The number of cells finally chosen is equal to 131x131 for α=0°, 173x173 for ±30° and 229x229 for ±60°. The time step taken for the simulation is 10 ms. Convergence is considered attained when the difference between two successive iterations is less than 10^{-6} for the temperature, energy and velocity components. Heat radiation is not considered (overall IR emissivity of all walls is set to zero). At the beginning of the calculation procedure, the entire cavity is supposed isothermal at T_0 and the velocity is zero everywhere. The air is assumed to be isotropic and all its properties are evaluated at the average temperature of each control volume. The 2D convective flow is assumed to be incompressible.

3. Results

Distributions of dimensionless viscous shear stress at hot wall τ^* are depicted in Fig. 2 for α=0, ± 30° and ± 60°, at *Ra*=1.48 x 10^6. Local values on the wall, denoted by *a* and *b*, are presented at two Fourier numbers Fo_1=0.048 and Fo_2=1.2. The first one is representative of the transient regime while the second one concerns the steady state. Average values on each band $\overline{\tau_i^*}$ (*i*=1-5) are indicated with vertical lines labelled as 1 and 2. Average values concerning the entire wall $\overline{\tau^*}$ are represented by vertical lines on the horizontal axis, labelled with A and B respectively for the two considered *Fo* numbers. For the right cavity (α=0) there is a regular increase in τ^* near the two lower active bands (1 and 2) and near the bottom of the upper active band 3. In these zones, the convective flow can be considered to be little influenced by the upper and lower walls of the enclosure. The shear stress decreases in the upper part of the active band 3 and becomes zero at the top of the wall, as expected. Adiabatic intermediate bands significantly affect the distribution of the wall shear stress. The lack of thermal activity on these bands reduces the local values of τ^* in transient and steady state regimes. The same trend is observed for "conducting" cavities (α>0). Convection, favored by these geometries, increases the local velocity gradient both on the active and adiabatic bands. Local values of τ^* are therefore higher than those concerning the right cavity. The adiabatic bands have less influence on the wall shear stress, having a smaller attenuation in the passive zones. Distributions of τ^* have a similar aspect for the two treated Fourier numbers. In the case of insulating cavities (α<0), the distribution is significantly different. For these geometries, the channel of the cavity is very narrow and the flow is reduced, the more the larger inclination angles. For α=-60°, τ^* is low and almost zero in the vicinity of the passive parts of the hot wall. Nonzero average values of viscous shear stress $\overline{\tau_i^*}$ in these areas are simply due to connections with upper and lower active zones. For α=-30°, the flow is more intense than for α=-60°, but it affects only the upper half of the plate in which there is an increase of the local and mean values of the viscous shear stress, including the adiabatic zone.

Average values of viscous shear stress $\overline{\tau_i^*}$ for the three active bands have the same trend as that of the Nusselt number, (see [12,14]). The increase of $\overline{\tau_i^*}$ is regular between α=-60° and +30° and decreases beyond this inclination angle, following the same pattern of the convective heat transfer within this type of cavities. The same goes for the average value over the entire hot wall, showing a good correlation between the flow dynamics and the thermal phenomena. For both Fourier numbers considered, the gap between the respective curves is substantial for insulating cavities, it is reduced for the right cavity and becomes very small for conducting ones. This is a valuable piece of information on the time required for establishing the steady state in diode cavities.

The analysis of the dynamic aspect is completed with the thermal one. Fig. 3 represents the dimensionless vertical temperature gradient at the hot wall $\frac{\partial T_h^*}{\partial y^*} = \left(\frac{\partial T^*}{\partial y^*}\right)_{x=0}$ for the same angles, *Fo* and *Ra* numbers mentioned above, with the same indications. The gradients are systematically higher at the junctions between active and adiabatic bands, due to juxtaposition of two different thermal conditions. The interpretation of the results is therefore done leaving these intersection areas aside. Distributions are significantly different from one configuration to another, depending on the local flow. For $\alpha \leq 0$, the gradients are systematically positive near the active zones. It is the same for both bands 1 and 2 for α=+30° and +60°. The gradient in the upper band is however characterized by different distributions for conducting cavities. Values are positive only in the lower part for α=+30°, being negative in the upper part. The gradient is always negative over the entire higher active band for α=+60°. This is due to the strong effect of the geometry on the features of the flow, especially for large inclinations. At α=+60° for example, only the upper part of the band 3 is affected by convective heat transfer due to the air flow coming from the cold wall. The gradients are mostly negative over the adiabatic bands of the hot wall for all the inclination angles. Absolute values tend to increase from the bottom to the top of these areas for $\alpha \geq 0$. On the contrary, they tend to decrease for insulating cavities. Finally, as observed previously for the viscous shear stress, the distributions of local temperature gradient at both Fourier numbers are clearly shifted for the insulating cavities and almost merge for $\alpha \geq 0$. The same applies to mean values for each band and for the entire wall. Dimensionless temperature T^* on the four walls of the cavity is of great interest for understanding the convective phenomena occurring in these parallelogram-shape cavities. This has been determined for all the studied configurations and is presented in Fig. 4 for the *Fo* and *Ra* numbers mentioned above. The figure provides useful information for the thermal design of cases containing electronic equipments. The wide variety of thermal states highlights the convective diode quality of these cavities and the values of T^* indicate the features of the flow. The observed superposition of transient and steady-state distributions for α=-60° for example, confirms the quasi stagnation of the flow and the thermal stratification of the fluid. Temperature and streamlines fields at Fo_1=0.048 and Fo_2=1.2 for α=±60° and Ra=1.48 x 10^6 are represented in Fig. 5. They provide additional information on the thermal and dynamic phenomena that occur in these cavities, as well as on the generated shear stress depending on the treated configuration.

A comparison has been done with measurements taken at steady state on a particular experimental setup whose details are given in [11] and summarized below. The cold wall is a copper plate maintained isothermal between -50°C and +10°C with an accuracy of ±0.1°C by means of an internal coolant fluid flow controled by a PID regulator. Its temperature T_c is measured in 3 points. The channel of the cavity is made of plates of extruded polyurethane

whose average thermal conductivity λ_{ch} is 0.041±0.007 $Wm^{-1}K^{-1}$ and of 60±2 mm in thickness. Surface temperatures are measured on both the internal and external sides of the channel. Given the considered 2D flow, measurements are taken on the centerlines of the top, bottom and one of the lateral walls. Four, eight and twelve thermocouples are installed for the three considered inclination angles α=0, ±30 and ±60° respectively. The hot wall shown in Fig. 6 (a) is made of a double sided PCB. The active part submitted to the fluid flow (H=191±2 mm; W=510±2 mm), consists on 5 superimposed horizontal bands. The top, bottom and intermediate bands represent the 3 active bands of the treated case while the two others represent the adiabatic ones. Each horizontal active band is formed by 5 juxtaposed electrical resistors connected in series. Each active band on one side is connected in series with its symmetrical one on the other side. Electrical resistances of the 3 active bands are equal, with a maximum deviation of about 0.2%. They are supplied in parallel with a stabilized power supply in order to accomplish the constant heat flux condition. Temperature T_h is measured at steady state in the central plane ($z^* = 0.5$) on the entire height H. Four measurements are done on every band on both faces what allows a proper determination of the vertical temperature gradient distribution. A guard resistor is laid out all around the active area in order to avoid lateral heat exchanges and also to ensure the 2D flow in the median plan of the cavity. Its thermal regulation is carried out at ±0.1°C by means of a PID regulator. The inner walls of the cavity (channel, hot and cold plates) are coated with a thin adhesive aluminum film whose total measured infrared emissivity ε=0.085±0.012 strongly reduces the radiative heat transfer. To eliminate the problem of the heat losses at the back of the hot wall, a symmetrical assembly consisting on two identical channels is placed at both sides of the same hot plate. Two cold walls are then used to close both cavities. The experimental assembly sketched in Fig. 6(b) is laid on a frame that allows to study successively the "conducting" configuration (α>0) and the "isolating" one (α<0) by a simple rotation around its y-axis.

The whole setup is installed in a room which temperature is controled at the average temperature of the flow inside the considered cavity. That strongly reduces the conductive losses through the walls of the channel. All surface temperatures are measured in steady state with an accuracy of ±0.1°C by means of 0.1mm K-type thermocouples. The electrical data (resistances and intensity of the current) providing the supplied heat flux are measured by means of a multimeter of 2 x 10^6 points. The maximum relative uncertainty is of 0.1% for resistances and the maximum absolute uncertainty is of 0.6 mA for the current. Electrical and thermal data are collected by a fast data acquisition system controlled by a computer. The sampling time is 50 ms in transient regime and 100 ms in steady-state (variation of all surface temperatures less than 0.3%).

A comparison between the measured and calculated temperature values at the inner surface of the wall has been done. An example is presented in Fig. 7 for the dimensionlesses wall temperature T^* of the cavity at steady state (Fo_2=1.2) for α=+30° and Ra=1.48 x 10^6. The deviation of about 3% on average is acceptable, confirming the validity of the adopted numerical model.

Acknowledgements

Many thanks to Baya Taalilоucht N'Leksar and Saïd N'Thnebdar for their constant assistance, for everything they have done.

4. Conclusion

Local distribution and evolution of viscous shear stress and vertical temperature gradients on the hot wall of diode cavities have been investigated. Different configurations have been presented in transient regime for a better understanding of the transient phenomena concerning natural convection occurring in 2D air filled parallelogramm-shape enclosures. The influence of the angle of inclination on these two parameters has been established. Effects due to the adiabatic bands that separate the active bands under constant heat flux have also been shown. The information offered is necessary for thermoregulation of electronic equipments when it is acquired through the junctions of thermocouples disposed in the fluid layer adjacent to the active hot wall. The numerical results, which are confirmed by surface thermal measurements, show the need of using regulation thermocouples of high sensitivity and suitably arranged.

References

[1] Y. Joshi, M. Baelmans, D. Copeland, C.J.M. Lasance, J. Parry, J. Rantala, Challenges in thermal modelling of electronics at the system level : summary of panel held at the Therminic 2000, Microelectronics Journal 32 (2001) 797-800

[2] S. Moghaddam, M. Rada, A. Shooshtari, M. Ohadi, Y. Joshi , Evaluation of analytical models for thermal analysis and design of electronic packages, Microelectronics Journal 34 (2003) 223–230

[3] R. Zhu, H. Ding, Y. Su, Y. Yang, Modeling and Experimental Study on Characterization Micromachined Thermal Gas Inertial Sensors, Sensors 2010, 10, 8304-8315; doi:10.3390/s10090830

[4] G. Saha, S. Saha, M.N. Hasan, Md.Q. Islam, Natural convection heat transfer within octogonal enclosure, IJE Transactions A: Basics 23 (2010) No. 1, 1-10

[5] F. Arpino, N. Massarotti, A. Mauro, High Rayleigh Number laminar-free convection in cavities: new benchmark solutions, Numerical Heat Transfer, Part B, 58: 73–97, 2010

[6] G. V. Kuznetsov, M. A. Sheremet, Conjugate natural convection in an enclosure with a heat source of constant heat transfer rate, International Journal of Heat and Mass Transfer 54 (2011) 260–268

[7] G. V. Kuznetsov, M. A. Sheremet, Conjugate natural convection in a closed domain containing a heat-releasing element with a constant heat release intensity, Journal of Applied Mechanics and Technical Physics, Vol. 51, No. 5, pp. 699–712, 2010

[8] N. Nithyadevi, P. Kandaswamy, S. Malliga Sundari, Magnetoconvection in a square cavity with partially active vertical walls: Time periodic boundary condition, International Journal of Heat and Mass Transfer 52 (2009) 1945–1953

[9] A. Baïri, J.-M. García de María, N. Laraqi, Importance of radiative heat exchange in 2D closed diode cavities applied to solar collectors and buildings, nternational Journal of Sustainable Energy 25, 1 (205) 33-34

[10] A. Baïri, Transient free convection in passive buildings using 2D air-filled parallelogram-shaped enclosures with discrete isothermal heat sources, Energy and Buildings 43 (2010) 366-373

[11] A. Baïri, J.-M. García de María, N. Laraqi, Transient natural convection in parallelogrammic enclosures with isothermal hot wall. Experimental and numerical study applied to on-board electronics, Applied Thermal Engineering 30 (2010) 1115-1125

[12] J.-M. García de María, A. Baïri, V.A.F. Costa, Empirical correlations at high Ra for free convection in 2D air-filled parallelogrammic enclosures with isothermal discrete heat sources, International Journal of Heat and Mass Transfer 53 (19–20) (2010) 3831–3838

[13] A. Baïri, E. Zarco-Pernia, J.-M. García de María, N. Alilat, N. Laraqi, F. Gutiérrez, Nusselt-Rayleigh correlations for free convection in 2D air-filled parallelogrammic enclosures with isothermal active walls, Heat Mass Trnsfer, DOI 10.1007/s00231-010-0750-z
[14] A. Baïri, E. Zarco-Pernia, N. Alilat, N. Laraqi, J.-M. García de María, I. Baïri, 2D transient natural convection in diode cavities. Electronic equipment under constant heat flux, internal report LTIE-GTE 2010-123
[15] S. Ostrach, An analysis of laminar free convection flow and heat transfer about a flat plate parallel to the direction of the generating body force, NASA Technical Report 1111, 1953
[16] B. Gebhart, Similarity solutions for laminar external boundary region flows, Natural Convection, Fundamentals and Applications, Hemisphere Publishing Corporation, Washington, 1985
[17] B. Gebhart, Effects of viscous dissipation in natural convection, J. Fluid Mech. 14 (1962) 225–232
[18] N. Nadim, G. Domairry, Analytical study of natural convection in high Prandtl number, Energy Conversion and Management 50 (2009) 1056–1061
[19] S. Sillanpää, M. Heinonen, The varying effect of natural convection on shear stress rate on cylindrical surfaces, Experimental Thermal and Fluid Science 32 (2007) 459–466
[20] S.V. Patankar, Numerical heat transfer and fluid flow, series in computational methods in mechanics and thermal sciences, W. J. Minkowycz and E. M. Sparrow Editors, Taylor and Francis Publishers, ISBN 0-89116-522-3, 1980
[21] H. Schlichting, Boundary-Layer Theory, 6th edition, Mc Graw Hill, Inc., LCCCN 67-29199, 1968

Highlights

This work examine the 2D transient natural convection generated by a working vertical electronic equipment vertical composed by alternated adiabatic and heated bands under constant heat flux. This equipment is contained in a parallelogram shaped air-filled cavity. Viscous shear stress that could affect thermocouples used for thermal regulation of these assemblies are determined by numerical approach and some measurements.

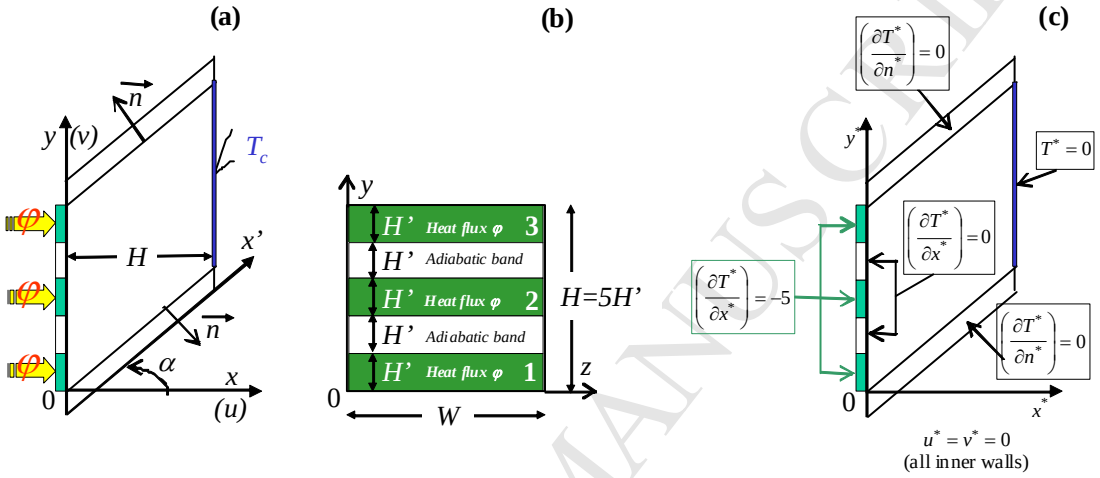

Fig. 1. The studied enclosure: (a) parallelogram-shaped cavity; (b) active hot wall; (c) the boundary conditions

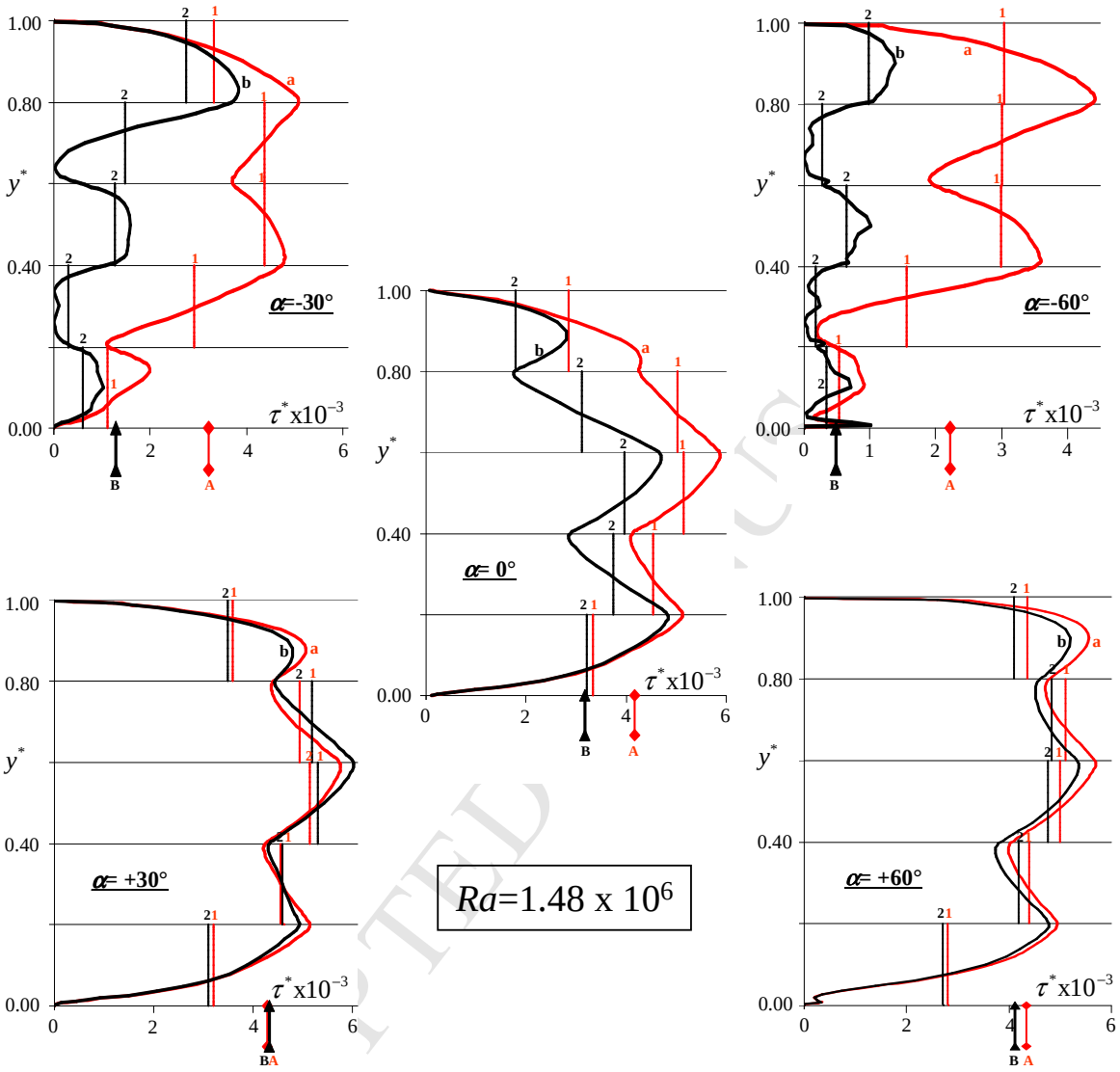

Fig. 2. Dimensionless viscous shear stress at the hot wall. Local distribution: curve *a* (Fo_1=0.048) and curve *b* (Fo_2=1.2). Average values on each band: vertical lines 1 and 2 for Fo_1 and Fo_2 respectively. Average values on the entire hot wall: lines A and B on the horizontal axis, for Fo_1 and Fo_2 respectively. Ra=1.48 x 10^6; α=0º, ± 30° and ± 60°.

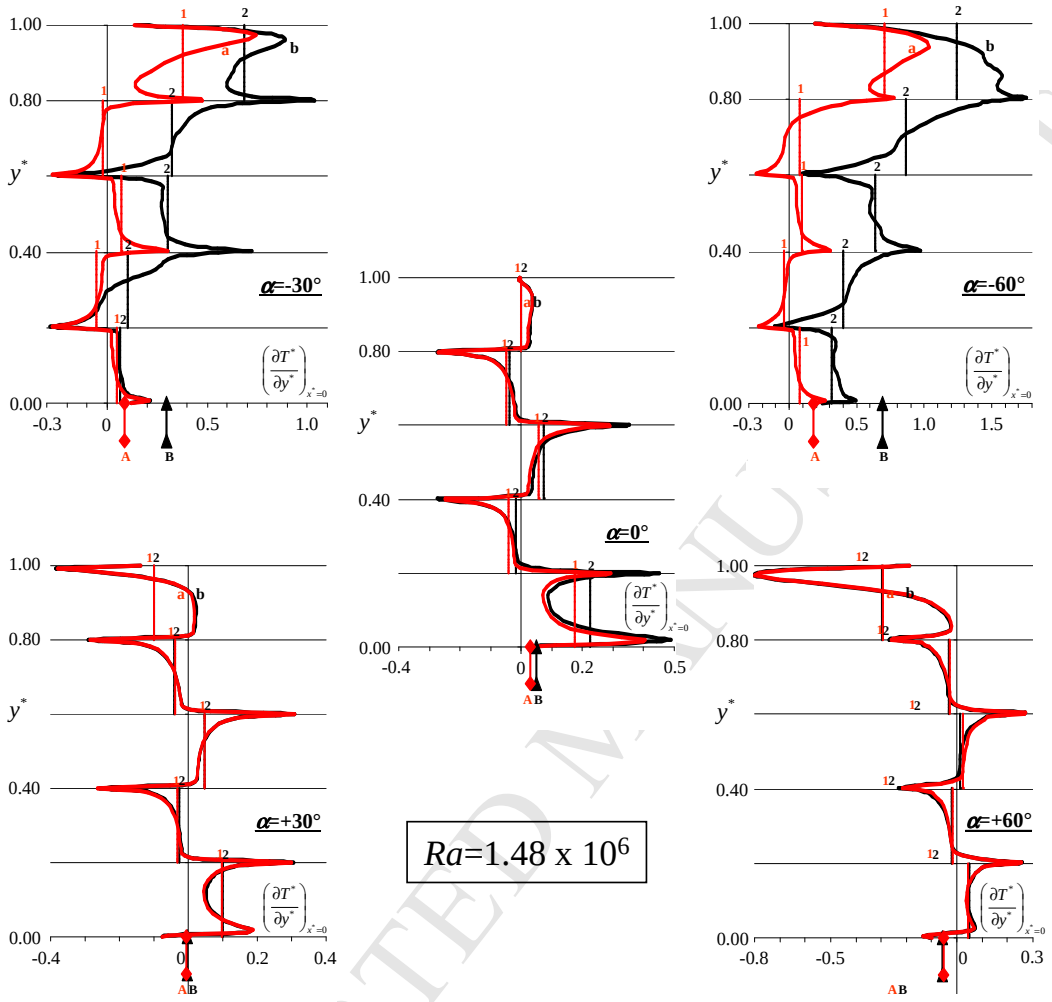

Fig. 3. Dimensionless vertical temperature gradient at the hot wall. Local distribution: curve a (Fo_1=0.048) and curve b (Fo_2=1.2). Average values on each band: vertical lines 1 and 2 for Fo_1 and Fo_2 respectively. Average values on the entire hot wall: lines A and B on horizontal axis, for Fo_1 and Fo_2 respectively. Ra=1.48 x 10^6; α=0º, ± 30° and ± 60°.

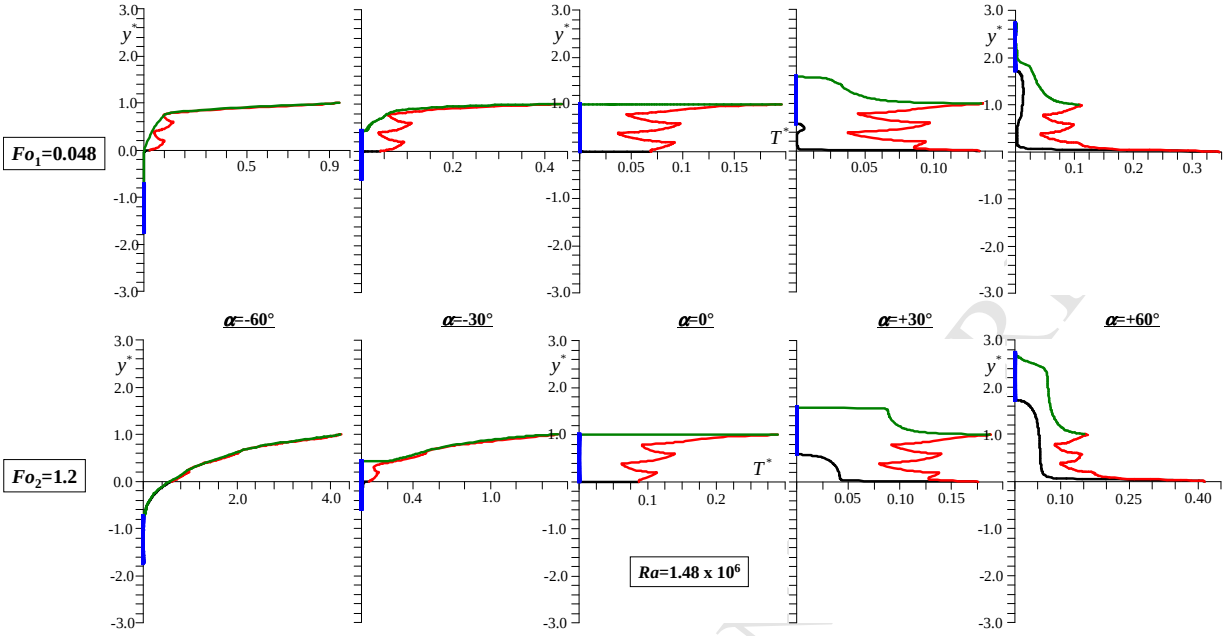

Fig. 4. Dimensionless temperature on the cavity walls for Fo_1=0.048 (upper row) and Fo_2=1.2 (lower row). Ra=1.48 x 10^6; α=0º, ± 30° and ± 60°. Cold wall (blue), hot wall (red), upper wall (green) and lower wall (black)

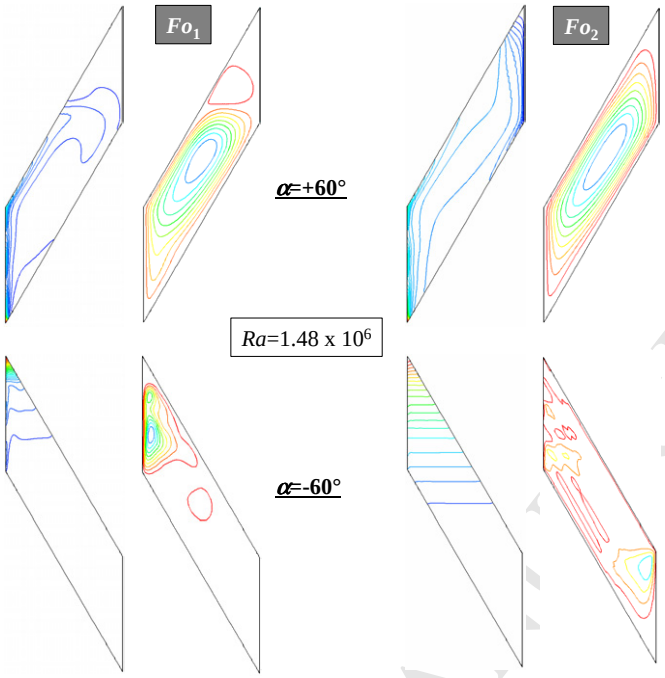

Fig. 5. Dimensionless temperature and streamlines fields at Fo_1=0.048 and Fo_2=1.2. α=±60° ; Ra=1.48 x 10^6.

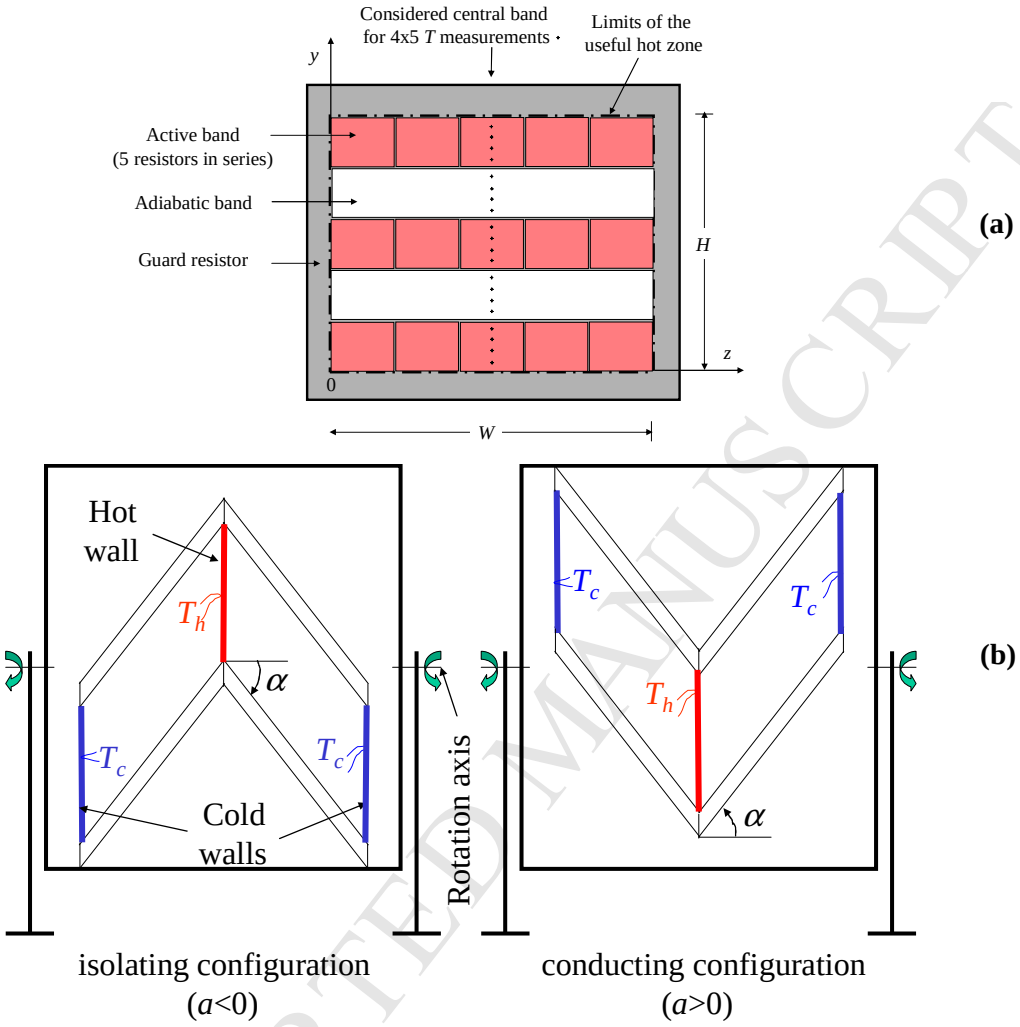

Fig. 6: Schematics of the hot wall (a) and the experimental setup (b)

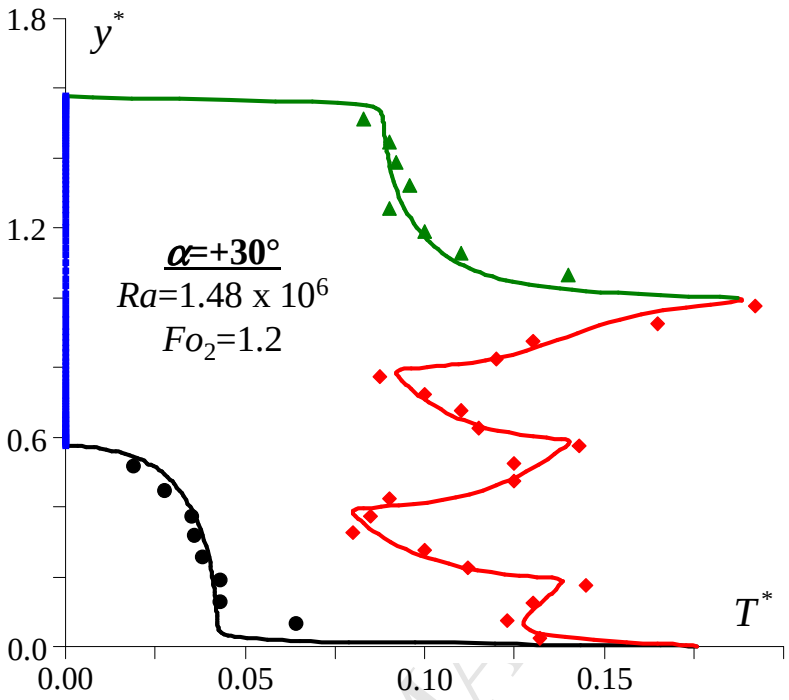

Fig. 7. Dimensionless temperature T^* of the inner wall at steady state (Fo_2=1.2) for α=+30° and Ra=1.48 x 10^6. Comparison between calculated (solid line) and measured (discrete points) values